IET Energy Systems Integration

Research Article

IET Journals
The Institution of Engineering and Technology

Microgrids interconnection to upstream AC grid using a dual-function fault current limiter and power flow controller: principle and test results

eISSN 2516-8401
Received on 31st January 2019
Revised 17th May 2019
Accepted on 16th June 2019
E-First on 5th August 2019
doi: 10.1049/iet-esi.2019.0014
www.ietdl.org

Nima Shafaghatian[1], Amir Heidary[2], Hamid Radmanesh[2] ✉, Kumars Rouzbehi[3]

[1]*Electrical Engineering Department, Zanjan University, Zanjan, Iran*
[2]*Electrical Engineering Department, Shahid Sattari Aeronautical University of science and technology, Tehran, Iran*
[3]*Department of System Engineering and Automatic Control, University of Seville, Seville, Spain*
✉ *E-mail: Radmanesh@ssau.ac.ir*

Abstract: This study presents a novel magnetic-based solid-state dual-function fault current limiter and power flow controller (FLPFC) that offers a promising application for safe and controllable interconnection of microgrids to upstream AC grids. The proposed structure includes series reactors and power electronic switches that protects microgrid from upstream AC grid short-circuit fault and it controls the power flow between microgrid and upstream grid. Performance of the proposed FLPFC is analysed and simulated using Matlab/Simulink and results are confirmed by experimental tests.

1 Introduction

In the past decade, power system community has found a practical way to integrate the emerged vast potential of distributed generations to grids by developing microgrids [1]. Actually, these small autonomic grids have existed for many decades in remote communities where the interconnection with the main power grid was not feasible due to technical and/or economic reasons. Due to their scalability, competitive investment costs and flexible operation, fossil-fuel generation technologies have been the most common choice for electricity supply in these remote grids. However, with the demonstrated technical and economic feasibility of greener generation technologies based on wind, solar, hydrogen, and hydropower, integrating these technologies has become a priority in microgrids [2]. Microgrids as sensitive distribution networks need to be carefully managed and protected against fault currents [3]. Solutions for the protection issues that have been reported in the literature are as follows: using a directional over-current relay, using differential protection schemes, using fault current limiters, protection based on negative and zero sequences, voltage-based protection, adaptive protection, and the coordinated protection techniques [3, 4]. Power management, intelligent control, and protection are the most critical factors for design and operation of efficient, reliable, and sustainable microgrids [5, 6]. Power flow can be adjusted by change in the line impedance or phase angle difference, or the bus voltages [7]. Power exchange control is studied in several small-scale systems using a power flow controller (PFC) [8]. The electric power flexibility control based on PFC hits several goals as follows: improved operation rate of regional renewable energies, reduced capacity, and increased use of accumulation of electrical equipment for electric power quality maintenance introduced into the system, improved supply reliability of renewable energies, advantage of scale for power generation equipment, and electricity storage equipment [8].

A type of variable inductor that can be controlled by DC bias flux which is generated by a DC current has been introduced in [9]. Its magnetic structure includes a series AC coil that connects an AC source to the load and the series reactor inductance is changed by DC flux in the core and consequently, AC current can be controlled as the PFC [10]. Actually, faults in the microgrid and upstream AC grids can damage grid apparatuses and its sensitive loads. In [11–15], fault current limiter (FCL) as a protection device in the microgrid is presented to limit the magnitude of the fault current. In [11], FCL is introduced as a solution for connecting upstream AC grid to the downstream microgrid. A resistive superconductor is a type of FCL that has been presented for preserving microgrid against faults [12]. In addition, solid-state FCLs are another type of fault limiters that have been reported in [13–15]. Solid-state FCLs are presented as a DC-reactor type FCL in [16], transformer-based solid-state overvoltage and current limiter [17], series transformer type FCL in [18, 19], AC/DC reactor type FCL in [20], and saturated core type FCL in [21–23]. Saturated core fault current limiter comprises of a DC bias coil and AC series coil where its core works both in saturation and linear states [22]. Recently, several novel magnetic-based topologies are introduced [23–25]. In [26], the saturated core FCL with two cores has been presented where DC coil did not influence the AC flux and negligible voltage induction appears on the DC coil.

In this paper, a novel magnetic-based power electronic device is presented to protect the microgrid against the fault current and is able to control the power exchange between the upstream AC grid and microgrid. The remaining parts of the paper are organised as follows:

Section 2 presents the system configuration and the proposed device structure. The analytical analysis is given in Section 3. Controlling unit is introduced in Section 4. Simulation results including current, voltage, and power waveforms are reported in Section 5. Experimental test results are reported in Section 6 and finally, conclusions are given in Section 7.

2 FLPFC configuration

This section presents the initial location and structural details of the proposed FLPFC. The proposed FLPFC is allocated in the tie-line connecting the microgrid to the upstream AC grid as shown in Fig. 1. In this location, power flow between the microgrid and upstream grid is controlled and both grids are protected against the grids fault currents from each other.

Fig. 2 shows the single line diagram of the proposed FLPFC structure comprises of two saturable cores, two AC windings, and a DC coil. Inductors L_{AC1} and L_{AC2} are located in separate cores 1 and 2. The device connected in series with the tie-line. The DC coil wrapped around both cores magnetic arm. Inductors L_{AC1} and L_{AC2} have equal inductance and those magnetic fluxes in the DC controlling core are reversed. Therefore, the AC flux passes through the DC coil is ∼0. The DC coil current and consequently

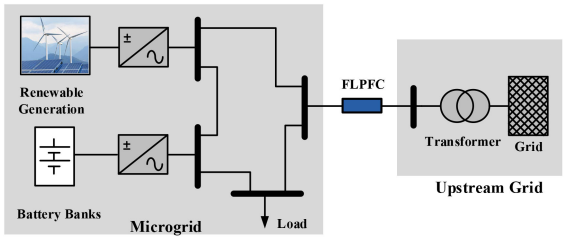

Fig. 1 *FLPFC placement in a grid*

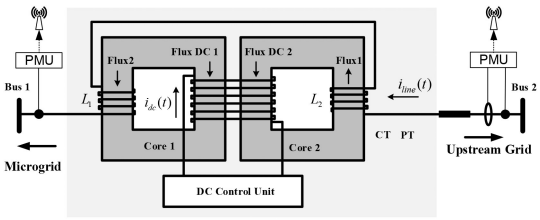

Fig. 2 *Proposed fault current limiter and power flow controller*

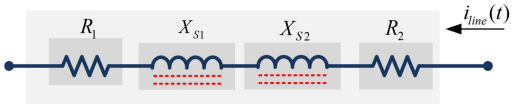

Fig. 3 *FLPFC equivalent circuit during normal mode*

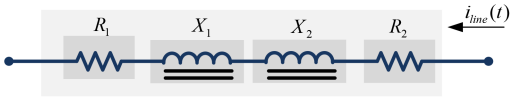

Fig. 4 *Proposed FLPFC equivalent circuit during fault mode*

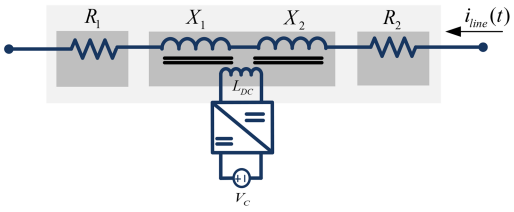

Fig. 5 *Proposed FLPFC equivalent circuit in PFC operation mode*

its DC flux is determined by DC controller unit, which acts according to the line current/voltage measurements.

The proposed structure operates in three operation modes. In the following, the equivalent circuit for each operation mode is presented and discussed. In the first operation mode, the grid is in normal operation and power flow control is not intended; therefore, the FLPFC presents a low series impedance. The second operation mode is dedicated to the grid faults. In this case, the fault current should be limited by high impedance. In the third operation mode, power flow control is carried out by impedance variation imposed by FLPFC.

2.1 Normal operation mode

During the normal operation mode, the DC coil saturates both cores to decrease the series AC reactor impedances. The equivalent circuit for this operation mode is shown in Fig. 3. In this equivalent circuit, X_{s1} and X_{s2} are the AC reactor impedances considering the magnetic leakages, R_1 and R_2 are coils resistors with negligible values.

2.2 Fault operation mode

During the fault condition, the line current increases suddenly. The fault current direction is dependent on the fault location i.e. AC upstream side or microgrid side. In the instant of upstream fault, the current transformer (CT) measures the line current and the control unit sends a command signal to the solid-state switches. In this case, the DC coil current interrupts and magnetic cores become saturated. Therefore, two series high-inductance AC reactors appear in the tie-line to limit the fault current and the proposed FLPFC protects the microgrid. Fig. 4 shows the equivalent circuit of the proposed FLPFC during the fault mode. In this circuit, X_1 and X_2 are the series reactor impedances while the magnetic core is not in the saturation region. R_1 and R_2 are the negligible resistance of the AC coil.

2.3 Power flow control mode

In this case, the FLPFC operates as a magnetic amplifier where the DC coil current acts as the control system and the AC coils produce a variable series inductance. In Fig. 5, it is shown that the value of X_1 and X_2 is controlled by the DC mutual effect of the DC inductor (L_{DC}). Note that, the DC inductor does not influence by AC coil because of those reverse coupling effect. In the magnetic core linear region, by increasing DC flux, AC coil impedance decreases and by falling the value of the DC flux, the AC coil impedance value is raised almost linearly. Therefore, the power flowing through the under control tie-line is controlled using the variable series impedance of the FLPFC. The variable DC current is provided by the power electronic variable source in the controlling system.

Comparing the proposed FLPFC and saturated core fault current limiters (SCFCLs), it is noteworthy to mention that, SCFCL just operates in two states. In the normal operation mode which its impedance is at minimum level by the core saturation action. In fault conditions, it protects networks by imposing maximum impedance where DC saturation current reaches to zero. Moreover, SCFCLs operate with a simple control mechanism just based on a fault detection system. In the proposed FLPFC, cores DC flux is controlled between zero till core saturation by the use of DC/DC converter. In this structure, power flow control is based on PMU measurements.

3 Analytical studies

In this section, analytical studies are given according to three equivalent circuits presented in Section 2. For this propose, three sets of separate equations are given to show properties of the proposed multi-functional FLPFC.

3.1 Normal operation mode

During the normal operation mode, the FLPFCL cores are completely saturated by the DC-biased coil. During the steady-state condition, the phasor analysis is applied to calculate the FLPFCL voltage drop and power losses as follows.

$$\boldsymbol{V}_{\mathrm{FLPFC}} = j(2\pi \mathrm{f})(L_{S1} + L_{S2})I_{\mathrm{line}} + (R_1 + R_2)I_{\mathrm{line}} \tag{1}$$

$$P_{\mathrm{loss(normal)}} = (R_1 + R_2)I^2_{\mathrm{line(normal)}} + R_{\mathrm{DC}}I^2_{\mathrm{DC}} \tag{2}$$

where $\boldsymbol{V}_{\mathrm{FLPFC}}$ is the voltage drop across the proposed device and depends on L_{S1} and L_{S2} as the leakage inductances of the AC coils, and R_1 and R_2 as the resistances of the AC coils. This voltage drop assumes to be negligible. In addition, $P_{\mathrm{loss(normal)}}$ depends on the square of the line current and DC saturation part current and DC and AC coil resistances where because of saturation state, core loss is zero.

3.2 Fault operation mode

In the fault conditions, the DC coil current reaches to zero, the FLPFC cores bring out the saturation region and AC coils inductance increases. During the fault period, we have the following equations.

$$v_{\mathrm{FLPFC}}(t) = (L_1 + L_2)\left(\frac{\mathrm{d}i_{\mathrm{line(fault)}}(t)}{\mathrm{d}t}\right) + (R_1 + R_2)i_{\mathrm{line(fault)}}(t) \tag{3}$$

$$i_{\text{line(fault)}}(t) = \frac{v_{\text{BUS1}}(t) - v_{\text{BUS2}}(t)}{\sqrt{\left((2\pi \text{f})^2(L_1 + L_2 + L_{\text{line}})\right)^2 + (R_1 + R_2 + R_{\text{line}})^2}} + I_{\max}\text{e}^{-(R_{\text{eq}}/L_{\text{eq}})t)} \quad (4)$$

$$P_{\text{loss(fault)}} = (R_1 + R_2)I^2_{\text{line(fault)}} + 2P_{\text{core}} \quad (5)$$

$$\frac{P_{\text{loss(fault)}}}{P_{\text{loss(normal)}}}\% = \frac{(R_1 + R_2)I^2_{\text{line(fault)}} + 2P_{\text{core}}}{(R_1 + R_2)I^2_{\text{line(normal)}} + R_{\text{DC}}I^2_{\text{DC}}} \times 100 \quad (6)$$

Equation (3) presents the FLPFC voltage drop which directly caused by high AC inductances L_1 and L_2 and the fault current $i_{\text{line(fault)}}$. In (4), line current in the fault mode is defined by the voltage difference between upstream and microgrid voltage and line impedance. The first term represents the steady-state current and the second term models the transient part. The peak value of the fault current depends on the fault location and equivalent resistance and inductance.

Equation (5) shows FLPFC power losses that depends on AC coils resistance, limited fault current, and cores loss. Equation (6) presents percentage ratio of power losses in the fault and normal operation condition.

3.3 PFC mode

Active power transfer between the upstream bus 1 and microgrid bus 2 is given by (7). As mentioned before, the transferred power can be controlled by an impedance change in the tie-line as shown in (8).

$$P_{\text{tr}} = \frac{V_a\, V_b}{X_T}\sin(\delta_{\text{ab}}) \quad (7)$$

$$X_T = (2\pi \text{f})(L_1 + L_2 + L_{\text{line}}) \quad (8)$$

where P_{tr} is active power transfer between upstream grid and microgrid. V_a and V_b are bus voltages, δ_{ab} is the phase angle difference and X_{line} is the line equivalent reactance.

Core specification is defined by its *B-H* curve. In (9), the proposed FLPFC *B-H* curve is modelled where $B_{\max}$ is saturation flux density, H_{DC} and H_{AC} are DC saturation and AC magnetising field is applied to the core. In (10), the FLPFC voltage drop is given where N_{AC} is the AC coil turns and A is core cross-section area. In (11), the FLPFC inductance value is shown depends on FLPFC AC and DC magnetising fields.

$$B_c(t) = B_{\max}(1 - \text{e}^{-(H_{\text{DC}} + H_{\text{AC}(t)})}) \quad (9)$$

$$v_{\text{FLPFC}}(t) = N_{\text{AC}}\text{AB}_{\max}\frac{\text{d}\left(1 - \text{e}^{-(H_{\text{DC}} + H_{\text{AC}(t)})}\right)}{\text{d}t} \quad (10)$$

$$L_{\text{FLPFC}} = \left(\frac{N_{\text{AC}}\text{AB}_{\max}}{\text{d}i_{\text{line}}(t)/\text{d}t}\right)\left(\frac{\text{d}\left(1 - \text{e}^{-(H_{\text{DC}} + H_{\text{AC}(t)})}\right)}{\text{d}t}\right) \quad (11)$$

Equation (12) presents the reactance value of the power flow controller and (13) models the transfer power based on DC bias current I_{DC}.

$$X_T = (\omega)\left\{\left(\frac{N \times A \times B_{\max}}{\text{d}i_{\text{line}}/\text{d}t}\right)\left(\text{e}^{(\xi \times I_{\text{DC}})}\right)\frac{\text{d}}{\text{d}t}\left(\text{e}^{-(\rho \times i_{\text{line}}(t))}\right) + L_{\text{line}}\right\} \quad (12)$$

Therefore, the transferred power is:

$$P_{\text{tr}} = \frac{V_a V_b \sin\delta}{\omega \text{k}\text{e}^{-(\xi \times I_{\text{DC}})}\text{e}^{-(\rho i_{\text{line}})} + \omega \text{L}_{\text{line}}} \quad (13)$$

where

$$k = N_{\text{AC}}A_C B_{\max} \quad (14)$$

$$\xi = \frac{N_{\text{DC}}}{l_c} \quad (15)$$

$$\rho = \frac{N_{\text{AC}}}{l_c} \quad (16)$$

As shown in (13), the transfer power is related to I_{DC}. The transfer power variation versus the DC coil current is shown in Fig. 6. In this curve, DC current changes between 0 and 50 A to provide DC flux and transfer power changes between a band limited by $X_{\text{line}} + X_{S1} + X_{S2}$ $X_{\text{line}} + X_1 + X_2$ and core saturation constrain. Moreover, in Fig. 6 the proposed FLPFC performance is presented considering three various phase angle differences due to upstream and microgrid generation condition. In fact, in order to transfer maximum power by FLPFC, we have some constraints that are leakage inductance of AC coils, line inductance and the other series impedance between the two networks. The minimum power transfer constraint is non-linear behaviour of the cores.

4 Control strategy

In this section, the control strategy is presented in three operation modes i.e. normal operation, fault limiting mode, and power flow controlling mode as shown in Fig. 7.

The buses voltage and current signals are sampled by the PMU units. Line voltage and current are compared with the reference current and voltage values to detect the fault or normal conditions. In the normal operation mode, the DC/DC converter feeds the maximum DC current for the cores saturation, and in the fault condition, the converter is turned-off and DC current reaches to zero. The power flow control mechanism can be activated by an external command, sent by the grid operator or dispatching centre. This system controls the DC/DC converter IGBTs pulse duty cycle by using current feedback to feed the appropriate DC current of the proposed FLPFC. The PFC control system has two inputs including DC control current and line power flow measurement. Moreover, power flow set-point handled by the communication layer changes converter DC current level to achieve new power flow set-point. To clarify more, control strategies of fault detection and power flow control are explained as follows:

4.1 Fault detection

In this control mode, line current and voltage are measured as data A and B. Data A is compared with the reference X and data B is compared with the reference Y. If A becomes >X or B becomes <Y, then fault state will be detected and, DC/DC converter PWM decreases to zero and its output DC current reaches zero. If not,

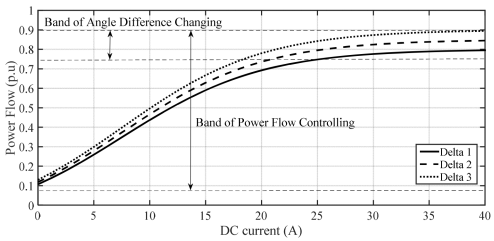

Fig. 6 *Transferred power as a function of controlling DC current*

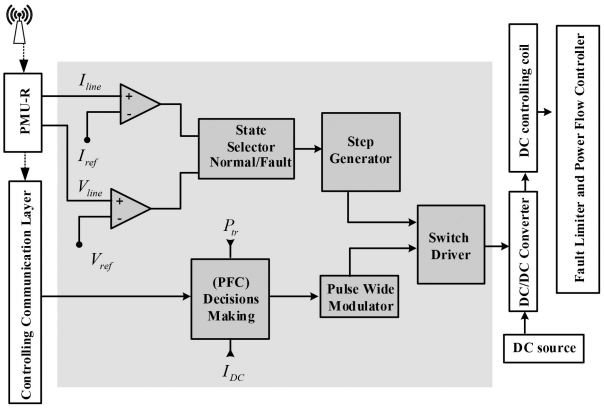

Fig. 7 *Control diagram of the proposed FLPFC*

Table 1 Electrical elements information

Parameter	Description	Value
V_a	microgrid bus voltage	1.02 pu
V_b	upstream bus voltage	9.9 pu
δ_{ab}	phase angle difference of voltages	7 deg
L_1	maximum inductance of first AC coil	0.2 H
L_2	maximum inductance of the second AC coil	0.2 H
L_{line}	tie- line inductance	10 mH
L_{DC}	DC saturation maximum inductance	1.5 H
R_{FCL}	FCL resistance	0.08 Ω
R_{line}	line resistance	0.05 Ω
R_{fault}	fault resistance	0.01 Ω
V_{base}	voltage base value	63 kV
I_{base}	current base value	500 A
S_{base}	apparent power base value	315 KVA

grid works in normal operation and DC/DC power converter PWM is in its initial setting.

4.2 Power flow control

In this control mode, local operator or dispatching centre sends an appropriate reference of power flow as data Z. In this state, line power is measured as data C. Data C is compared with data Z. If C is >Z, then generated command decreases DC/DC power converter PWM to decrease DC control current. If not, data C is <Z, then generated command increases DC/DC power converter PWM to increase DC control current. Accordingly, power flow can be adjusted to data Z.

5 Simulation result

In this section, simulation results are carried out considering two cases i.e. fault current limiting mode and power flow controlling mode. In the first case, the fault is applied to the upstream grid and microgrid forced to supply considerable fault current. Therefore, effect of the proposed FLPFC is studied for microgrid protection in the fault condition mode. In the next case, the power flow is controlled and fixed in two levels. Simulation is done based on the proposed grid shown in Fig. 1 and the electrical parameters values are listed in Table 1. The results are given in per unit, and the base values are presented in Table 1.

5.1 Fault current limiter mode

It is assumed that the fault has occurred in the upstream grid. In this case, 40% of microgrid demanded power is provided by the upstream grid and 60% of the power is provided by the microgrid distributed generators (DGs). Fault location is considered to be 20 km far from bus 2 in the upstream grid, which cause a very high voltage drop in this bus. Due to the occurred fault, the fault current is flowed by microgrid generators. Fig. 7 shows voltage, current, and power flow during the normal and fault conditions are affected by the proposed FLPFC.

Fig. 7*a* shows the microgrid bus 1 voltage during the normal and fault conditions while its normal value is 1 p.u. The fault has occurred in $t = 100$ ms and microgrid voltage is restored and fixed to 0.92 p.u, after a transient state. In Fig. 7*b*, the upstream bus 2 voltage is presented while fault has occurred in upstream close to bus 2. During the normal operation, the bus voltage is almost 1 p.u and in the faulty condition high voltage sag occurs and its amplitude decreases to 0.2 p.u. Fig. 7*c* shows the proposed the FLPFC voltage drop. As shown here, there is a negligible voltage drop during the normal operation mode because the magnetic core is completely saturated. In this state, its voltage drop reaches to 0.02 p.u but after fault occurrences and interrupts of DC saturation current, its voltage drop raised to 0.87 p.u and protects the microgrid from upstream fault. The current waveform is shown by Fig. 7*d* while during the normal operation mode, its amplitude is 0.65 p.u from the upstream to the microgrid. In the fault duration, the limited current with 0.8 p.u amplitude is sent from the microgrid to the fault location. Fig. 7*e* shows the power flow between the upstream and the microgrid. In the normal operation mode, the upstream sends ∼0.4 p.u active power to the microgrid and after the fault occurrences, the power flow is limited by the proposed FLPFC and reaches to <0.1 p.u. Furthermore, the reactive power flow during the normal operation mode is 0.04 p.u.

5.2 Power flow control mode

In this case, the transferred power between the upstream and the microgrid is set in three different levels and performance of the proposed FLPFC in the power flow control mode is studied. From t_0 till t_1, the power flow is set in the first setup. From t_1 till t_2 and t_2 till t_3, the power flow adjusts in the second and third setups. These

adjustable setups are resulted by variation of the DC control current. In Fig. 8*a*, the microgrid bus 1 voltage and the upstream bus 2 voltage are shown together and the power flow control factor is inductive impedance between these two voltages.

In Fig. 8*b*, FLPFC voltage drop is shown in the three separate setups. These setups are based on series reactor value changing which is given in (5). In each setup, L_1 and L_2 are changed by the DC control coil in agreement with (9). In the first setup, the FLPFC voltage drop is 1.1 p.u. In the second and third setups, the FLPFC voltage drop changes to 0.09 and 0.03 p.u, respectively. In Fig. 8*c*, the main signal is given presented the variable power flow in the line. In the first setup, the power flow is limited in 0.08 p.u. In the next setup, after a transient time i.e.10 ms, the power flow is fixed to 0.15 p.u. In the final setup and after a transient time, the power flow reaches to 0.35 p.u. This operation confirms the prospered operation of the FLPFC in PFC mode.

The value of required DC control current is not too much. As magneto motive force (mmf) for saturation is provided by DC coil turns and current (high numbers of coil turns and low current). On the other hand, resistance of the DC control coil is low. Therefore, a low voltage can feed acceptable DC current. Considering the explained operation, converter input power is low and magnitude of its current harmonic is low too. Furthermore, because of DC saturation coil low resistance and high inductance, DC current ripple is close to zero, which no series voltage harmonic is induced in AC coils.

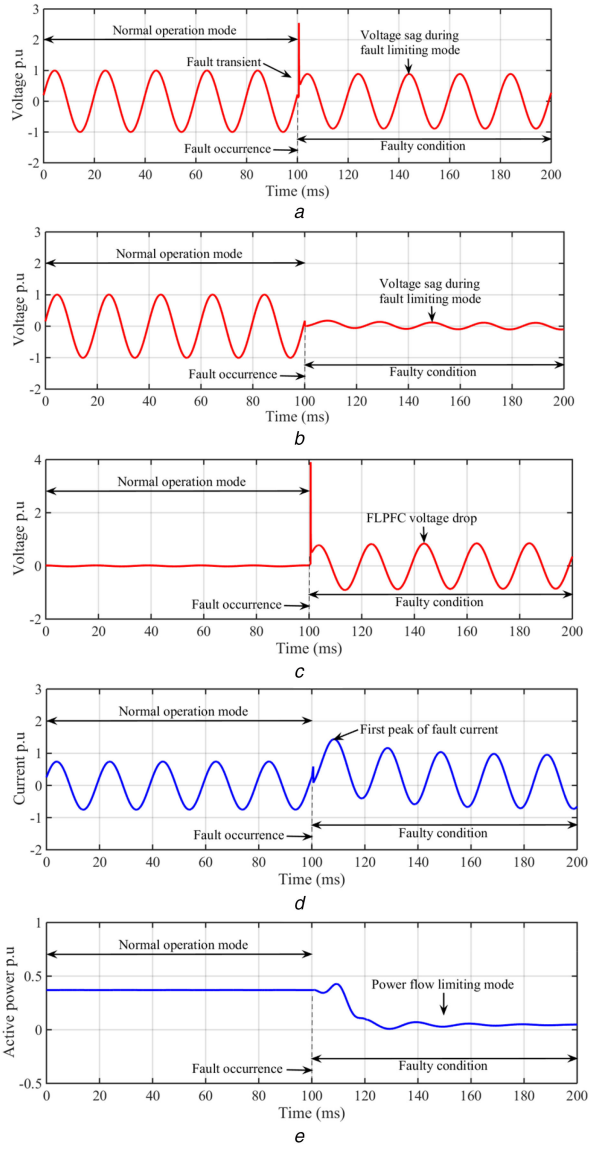

Fig. 8 *Fault limiting mode*
(a) Microgrid bus voltage, ***(b)*** Upstream bus voltage, ***(c)*** FLPFC voltage drop, ***(d)*** Line current, ***(e)*** Transferred active power

6 Experimental test result

In this section, the scaled-down experimental setup of the proposed PFCCL shown in Fig. 9 is tested and its results are presented. The laboratory setup parameter values are listed in Table 2, and Table 3 lists the electrical elements specifications.

In this prototype setup, the proposed PFCCL is connected between single-phase AC grid and microgrid that contains battery storage and inverter. In this laboratory experiment, the line current and the power flow signal are observed in two different tests. In the first test, fault is applied to the AC grid by using a solid-state relay. The impedance of fault is 0.01 Ω, and it is located between phase and ground. The line current and the power flow signal are measured as shown in Figs. 10*a* and *b*. It is clear that the fault current and the power flow is limited during faulty condition by fault current limiting operation, and it is in fair agreement with simulation results reported in Fig. 8. In the second test, there is no faulty condition and power flow is controlled by three different set-points. In Fig. 10*c*, power flow signal is shown where power flow values change. This result confirms simulations reported in Fig. 11.

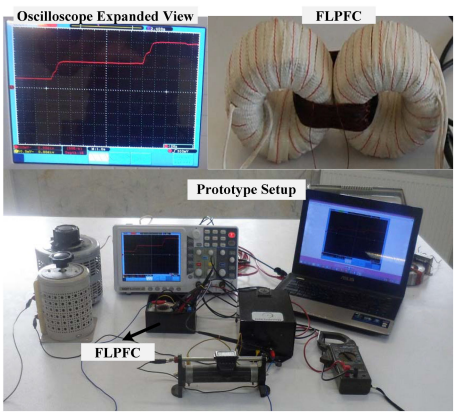

Fig. 9 *Experimental prototype setup*

Table 2 Electrical parameters values

Parameter	Description	Value
V_a	voltage of microgrid bus	16 V
V_b	voltage of upstream bus	15.9 V
δ_{ab}	phase angle difference of voltages	7 deg
L_1	maximum inductance of first AC coil	0.1 H
L_2	maximum inductance of the second AC coil	0.1 H
L_{line}	tie-line inductance	5 mH
L_{DC}	DC saturation maximum inductance	0.7 H
R_{line}	line resistance	0.01 Ω
R_{fault}	fault resistance	0.01 Ω

Table 3 Electrical elements data

Element	Description
core	toroid core, Fe powder
power converter	5–300 V DC/DC 1000 W
IGBT	STGP10NC60H
controller	NodeMCU
solid-state relay	30 A, 700 V

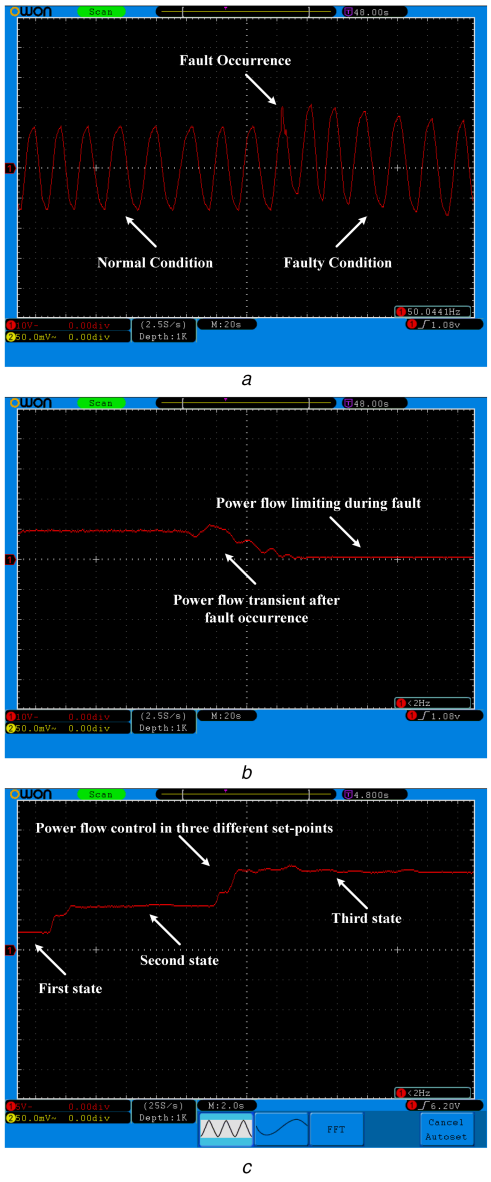

Fig. 10 *Experimental test results*
(a) Normal and fault current, ***(b)*** Power flow during normal and fault operation condition, ***(c)*** Power flow control during normal operation

7 Conclusion

In this paper, a novel magnetic-based solid-state dual-function FLPFC is presented. Its normal and fault operation modes are mathematically analysed, and its performance is validated with simulation and experimental prototype results. It is shown that this device offers a promising application for safe and controllable interconnection of the microgrids to the upstream AC grids. According to the analysis, the proposed FLPFC can successfully limit the microgrid overcurrent due to the upstream faults and is able to control the power flow between the upstream and the microgrid in a specified band.

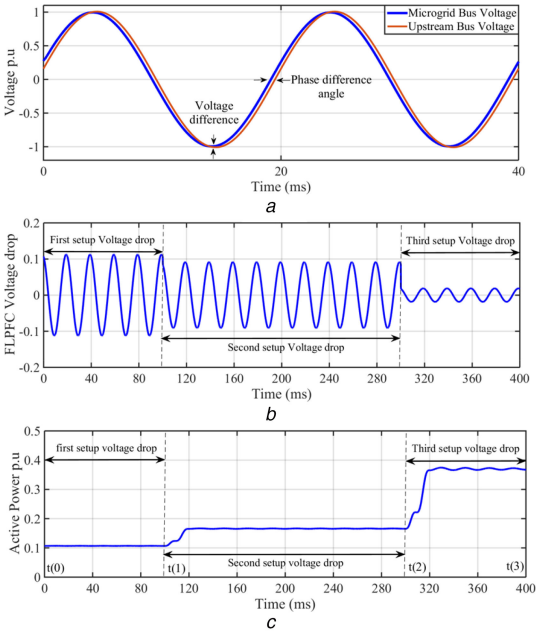

Fig. 11 *Simulation results in PFC mode*
(a) Bus bars voltage, ***(b)*** FLPFC voltage drop, ***(c)*** Active power flow

8 References

[1] Liu, X., Wang, P., Loh, P.C.: 'A hybrid AC/DC microgrid and its coordination control', *IEEE Trans. Smart Grid*, 2011, **2**, (2), pp. 278–286

[2] Olivares, D.E., Mehrizi-Sani, A., Etemadi, A.H., *et al.*: 'Trends in microgrid control', *IEEE Trans. Smart Grid*, 2014, **5**, (4), pp. 1905–1919

[3] Khademlahashy, A., Li, L., Every, J., *et al.*: 'A review on protection issues in micro-grids embedded with distribution generations'. 2017 12th IEEE Conf. on Industrial Electronics and Applications (ICIEA), Siem Reap, 2017, pp. 913–918

[4] Kang, X., Nuworklo, C.E.K., Tekpeti, B.S., *et al.*: 'Protection of micro-grid systems: a comprehensive survey', *J. Eng.*, 2017, **2017, (13)**, pp. 1515–1518

[5] Hooshyar, A., Iravani, R.: 'Microgrid protection', *Proc. IEEE.*, 2017, **105**, (7), pp. 1332–1353

[6] Vilathgamuwa, D.M., Loh, P.C., Li, Y.: 'Protection of microgrids during utility voltage sags', *IEEE Trans. Ind. Electron.*, 2006, **53**, (5), pp. 1427–1436

[7] Yuan, Z., de Haan, S.W.H., Ferreira, J.B., *et al.*: 'A FACTS device: distributed power-flow controller (DPFC)', *IEEE Trans. Power Electron.*, 2010, **25**, (10), pp. 2564–2572

[8] Sakai, T., Takeda, T., Yukita, K., *et al.*: 'Power exchange using PFC for micro grid'. 2014 Int. Power Electronics Conf., Hiroshima, 2014

[9] Hsu, J.W., Hu, A.P., Swain, A., *et al.*: 'A new contactless power pick-up with continuous variable inductor control using magnetic amplifier'. 2006 Int. Conf. on Power System Technology, Chongqing, China, 2006

[10] Austrina, L., Krah, J.H., Engdahl, G.: 'A modeling approach of a magnetic amplifier', *J. Magn. Magn. Mater.*, 2004, **272–276**, pp. 1709–1710

[11] Ghanbari, T., Farjah, E.: 'Unidirectional fault current limiter: an efficient interface between the microgrid and main network', *IEEE Trans. Power Syst.*, 2013, **28**, (2), pp. 1591–1598

[12] Zheng, F., Deng, C., Chen, L., *et al.*: 'Transient performance improvement of micro-grid by a resistive superconducting fault current limiter', *IEEE Trans. Appl. Supercond.*, 2015, **25**, (3), pp. 1–5

[13] Chen, L., Chen, H., Yang, J., *et al.*: 'Comparison of superconducting fault current limiter and dynamic voltage restorer for LVRT improvement of high penetration micro-grid', *IEEE Trans. Appl. Supercond.*, 2017, **27**, (4), pp. 1–7

[14] Ghanbari, T., Farjah, E.: 'Development of an efficient solid-state fault current limiter for microgrid', *IEEE Trans. Power Deliv.*., 2012, **27**, (4), pp. 1829–1834

[15] Madani, S.M., Rostami, M., Gharehpetian, G.B., *et al.*: 'Inrush current limiter based on three-phase diode bridge for Y-yg transformers', *IET Power Appl.*, 2012, **6**, (6), pp. 345–352

[16] Radmanesh, H., Heidary, A., Fathi, S.H., *et al.*: 'Dual function ferroresonance and fault current limiter based on DC reactor', *IET Gener. Transm. Distrib.*, 2016, **10**, (9), pp. 2058–2065

[17] Heidary, A., Radmanesh, H.: 'A novel smart solid-state ferroresonance limiter for voltage transformers', *IET Power Electron.*, 2018, **11**, (15), pp. 2545–2552
[18] Heidary, A., Radmanesh, H., Fathi, H.*, et al.*: 'Series transformer based diode-bridge-type solid state fault current limiter', *Frontiers of Inf. Tech. Electron. Eng.*, 2015, **16**, (9), pp. 769–784
[19] Zhang, X., Zhang, Y.: 'A viable approach for limiting fault currents in electric networks', *IEEJ Trans. Electr. Electron. Eng.*, 2018, **14**, (4), pp. 556–560, doi.org/10.1002/tee.22838
[20] Radmanesh, H., Fathi, S.H., Gharehpetian, G.B.*, et al.*: 'Bridge-type solid-state fault current limiter based on AC/DC reactor', *IEEE Trans. Power Deliv.*., 2016, **31**, (1), pp. 200–209
[21] Rozenshtein, V., Friedman, A., Wolfus, Y.*, et al.*: 'Saturated cores FCL – a new approach', *IEEE Trans. Appl. Supercond.*, 2007, **17**, (2), pp. 1756–1759
[22] Cvoric, D., Walter, S., De, H.*, et al.*: 'New saturable-core fault current limiter topology with reduced core size', *IEEJ Trans. Electr. Electron. Eng.*, 2011, **6**, (2), pp. 120–126
[23] Moriconi, F., De La Rosa, F., Darmann, F.*, et al.*: 'Deployment of saturated-core fault current limiters in distribution and transmission substations', *IEEE Trans. Appl. Supercond.*, 2011, **21**, (3), pp. 1288–1293
[24] Heidary, A., Radmanesh, H., Rouzbehi, K.*, et al.*: 'A DC-reactor based solid-state fault current limiter for HVDC applications', *IEEE Trans. Power Deliv.*, 2019, **34**, (2), pp. 720–728, 10.1109/TPWRD.2019.2894521
[25] Zhao, Y., Saha, T.K., Krause, O.*, et al.*: 'Current limiting impedance comparison between different designs of iron cores of the flux-lock-type superconducting fault current limiter', *IET Gener. Transm. Distrib.*, 2016, **10**, (2), pp. 548–554
[26] Sadeghi, M.H., Damchi, Y., Shirani, H.: 'Improvement of operation of power transformer protection system during sympathetic inrush current phenomena using fault current limiter', *IET Gener. Transm. Distrib.*, 2018, **12**, (22), pp. 5968–5974